PNAS RESEARCH ARTICLE | IMMUNOLOGY AND INFLAMMATION OPEN ACCESS

Central TYK2 inhibition identifies TYK2 as a key neuroimmune modulator

Tyler P. Molitor[a,1], Genki Hayashi[a], Mei-Yao Lin[a], Carissa J. Dunn[a], Nathan G. Peterson[a], Robert G. Poston[a], Michael P. Kurnellas[a], David A. Traver[a], Seona Patel[a], Zeynep Akgungor[a], Virginia Leonardi[a], Colizel Lewis[a], Joshua S. Segales[a], Dylan S. Bennett[a], Anh P. Truong[b], Manjari Dani[a], Swati Naphade[a], Jamie K. Wong[c], Annie E. McDermott[c], Sarah M. Kovalev[c], Gillian L. Ciaccio[c], Saud A. Sadiq[c], Zhonghua Pei[b], Stephen Wood[a], and Arash Rassoulpour[a,1]

Edited by Lawrence Steinman, Stanford University Beckman Center for Molecular and Genetic Medicine, Stanford, CA; received November 15, 2024; accepted February 3, 2025

GWAS have identified tyrosine kinase 2 (TYK2) variants in multiple inflammatory disorders, specifically a protective hypomorphic TYK2 allele (P1104A) in multiple sclerosis (MS). Impaired TYK2 signaling within the central nervous system (CNS) may impart the protective effects of TYK2 P1104A allele in MS. We deployed brain-penetrant TYK2 inhibitors (cTYK2i) alongside the peripherally restricted TYK2 inhibitor (pTYK2i; BMS-986165) to untangle the contributions of central TYK2 inhibition in diverse models of neuroinflammation. While pTYK2i had little impact, cTYK2i reduced clinical score, lymphoid cell infiltration, and cytokines/chemokines in experimental autoimmune encephalomyelitis (EAE). Microglial activation was attenuated in cTYK2i-treated EAE spinal cords and circulating neurofilament light (NfL) was reduced in plasma and cerebral spinal fluid (CSF). Additionally, cTYK2i was protective in an antibody-mediated mouse model of primary progressive MS (PPMS). Finally, we demonstrate TYK2 inhibition has a robust impact on a unique subset of activated astrocytes termed Interferon-Responsive-Reactive-Astrocytes (IRRA). The data presented herein identify a key role for CNS TYK2 signaling in regulating neuroinflammation and solidify TYK2 as a potential therapeutic target for MS.

neuroinflammation | autoimmunity | EAE | TYK2 | glial cells

Significance

TYK2 inhibitors were proven to be potent modulators of autoimmune disorders. We have developed selective centrally penetrant TYK2 inhibitors that can modulate the pathogenesis of neuroinflammation in EAE (a preclinical model of MS) in ways peripherally restricted TYK2 inhibitors fall short. The mechanisms presented here strengthen the strategy for targeting TYK2 in the central compartment for treatment of MS.

TYK2 is a member of the Janus Kinase (JAKs) of nonreceptor tyrosine kinases that mediates intracellular signaling and cellular responses to growth factors and cytokines. The JAKs (JAK1, JAK2, JAK3 and TYK2) phosphorylate signal transducer and activator of transcription (STAT) factors to regulate multiple inflammatory pathways, and the dysfunction of these pathways are linked to disease (1). TYK2 has a distinct role in the regulation of signaling through type I IFN, IL-12, IL-23, and IL-10 families as well as IL-4/IL-13, and IL-6 cytokines (2). TYK2-directed regulation of immune cell function plays an important role in multiple inflammatory disorders like psoriasis, systemic lupus erythematosus (SLE), rheumatoid arthritis, ankylosing spondylitis, ulcerative colitis, and MS. As such, many explored genetic disturbances in TYK2 as a potential driver of inflammatory diseases, and this work led to the identification of both loss of function and gain of function mutations in TYK2 (3, 4). Investigation of therapeutic modification of TYK2 activity has led to the development of small molecule inhibitors of TYK2 for autoimmune diseases, including the approval of Deucravacitinib for the treatment of psoriasis (2, 5).

The role of TYK2 in peripheral immune function and disease is well described. Despite expression in all CNS cell types (6), little is understood about the role of TYK2 in the CNS. Genome-wide association studies (GWAS) have identified a single nuclear polymorphism (rs34536443) associated with multiple autoimmune diseases including those of the CNS, such as MS (7, 8). The encoded human missense variant (P1104A) results in decreased TYK2 activity imparting protection in multiple inflammatory disorders by impairing type I IFN and IL-12/23 signaling (8–10). Transgenic mice that were *Tyk2* null or harboring the orthologous rs34536443 missense (P1124A) variant demonstrated protective effects in autoimmune disorders including mouse models of MS. Both *Tyk2* KO mice and TYK2 P1124A homozygous mice were protected from experimental autoimmune encephalomyelitis (EAE), showed T helper 1 (Th_1) and T helper 17 (Th_{17}) impairment, as well as reduced $CD4^+$ T cell infiltration in the CNS (10–12). While powerful, these models could not segregate the impact of peripheral vs central TYK2 signaling on EAE pathogenesis. Additionally, deployment of peripherally restricted TYK2 inhibitor (BMS-986165) was shown to be protective in multiple models of autoimmune disorders thereby recapitulating the protective effects of P1104 allele, yet EAE was not examined

Author affiliations: [a]Department of Biology, Neuron23, Inc., South San Francisco, CA 94080; [b]Department of Chemistry, Neuron23, Inc., South San Francisco, CA 94080; and [c]Tisch MS Research Center of New York, New York, NY 10019

Author contributions: T.P.M., G.H., M.-Y.L., C.J.D., N.G.P., R.G.P., M.P.K., S.N., J.K.W., S.A.S., S.W., and A.R. designed research; T.P.M., G.H., M.-Y.L., C.J.D., N.G.P., R.G.P., D.A.T., S.P., Z.A., V.L., C.L., J.S.S., D.S.B., A.P.T., M.D., J.K.W., A.E.M., S.M.K., and G.L.C. performed research; A.P.T. and Z.P. contributed new reagents/analytic tools; T.P.M., G.H., M.-Y.L., C.J.D., N.G.P., R.G.P., M.P.K., S.P., J.K.W., A.E.M., S.M.K., and G.L.C. analyzed data; and T.P.M., G.H., M.-Y.L., C.J.D., R.G.P., and M.P.K. wrote the paper.

Competing interest statement: Excluding J.K.W., A.E.M., G.L.C., S.M.K., and S.A.S., all remaining authors are employees of Neuron23, Inc. a for profit company. Neuron23, Inc. funded most of the research presented within. Experiments performed in collaboration with the Tisch MS Research Center of New York were executed by Tisch Researchers and funded by Tisch internal funds. Neuron23 Inc. holds the following patents as it relates to compounds that modulate the activity of one or more kinases, such as TYK2 or mutants thereof: US-20230373985-A1, US-20240025906-A1, US20240067655-A1. Characterization of chemical compounds utilized in this study can be found within US patents: US-20230373985-A1, US-20240025906-A1, US-20240067655-A1.

This article is a PNAS Direct Submission.

[1]To whom correspondence may be addressed. Email: tyler.molitor@neuron23.com or arash.rassoulpour@neuron23.com.

This article contains supporting information online at https://www.pnas.org/lookup/suppl/doi:10.1073/pnas.2422172122/-/DCSupplemental.

Published March 24, 2025.

(13). We hypothesized that impaired TYK2 signaling within the CNS plays a key role in the protective effects of the TYK2 P1124A allele in the EAE model.

Aligning with the "inside-out hypothesis" of smoldering neuroinflammation (14, 15), we sought to build an understanding of the underlying mechanisms of TYK2's function in the CNS using our selective and brain penetrant TYK2 inhibitors (cTYK2i). In this study, we demonstrated conserved function of TYK2 signaling in iPSC-derived glial cell populations and translated this mechanism to in vivo models of neuroinflammation to demonstrate functional potency of our cTYK2i. We deployed our cTYK2i alongside the pTYK2i, BMS-986165, in diverse forms of EAE to disentangle the contributions of CNS TYK2 inhibition in modifying EAE pathophysiology. We demonstrate inhibiting TYK2 within the CNS is essential for maximizing protective effects by reducing neuroinflammation and identify clear impact on reactive glial cell populations through central TYK2 inhibition. Furthermore, we show central TYK2 inhibition extinguishes key neuroinflammatory mechanisms, NF-κB signaling, and cytokine/chemokine production. Finally, we demonstrate related impacts on iPSC-derived astrocytes (iAstrocyte) whereby TYK2 inhibition quells chemokine expression and the reactive and neuroinflammatory signature from a unique population of reactive astrocytes, Interferon-Responsive-Reactive-Astrocytes (IRRAs). Ultimately, the data presented herein suggest a key role for TYK2 signaling within the CNS responsible for regulating neuroinflammation.

Results

Selective Inhibitors of TYK2 Abolish IFNα Stimulated Signaling in iPSC-Derived Astrocytes and Microglia. In vitro characterization of the potency and selectivity of a small molecule inhibitor of TYK2 can be accomplished by measuring levels of phosphorylated STATs (pSTAT) in response to cytokine stimuli (13, 16). We measured pSTAT5 abundance in THP-1 cells treated with IFNα and varying concentrations of several TYK2 inhibitors (n ≥ 7). The resulting IC_{50}s were 6.4, 2.9, and 1.2 nM for Compound -A (Cmpd-A), Compound-B (Cmpd-B), and BMS-986165, respectively (Fig. 1 *A*–*C*). Table 1 summarizes the potency of our compounds to inhibit TYK2-signaling from multiple stimuli and within diverse cell types. Compound selectivity profiles against other JAK family members were measured via IL-6-induced pSTAT3 (17, 18) and GM-CSF-induced pSTAT5 abundance (19, 20); IC_{50}s summarized in Table 1. Overall, Cmpd-A and Cmpd-B exhibit low nanomolar IFNα -pSTAT5 potency, similar

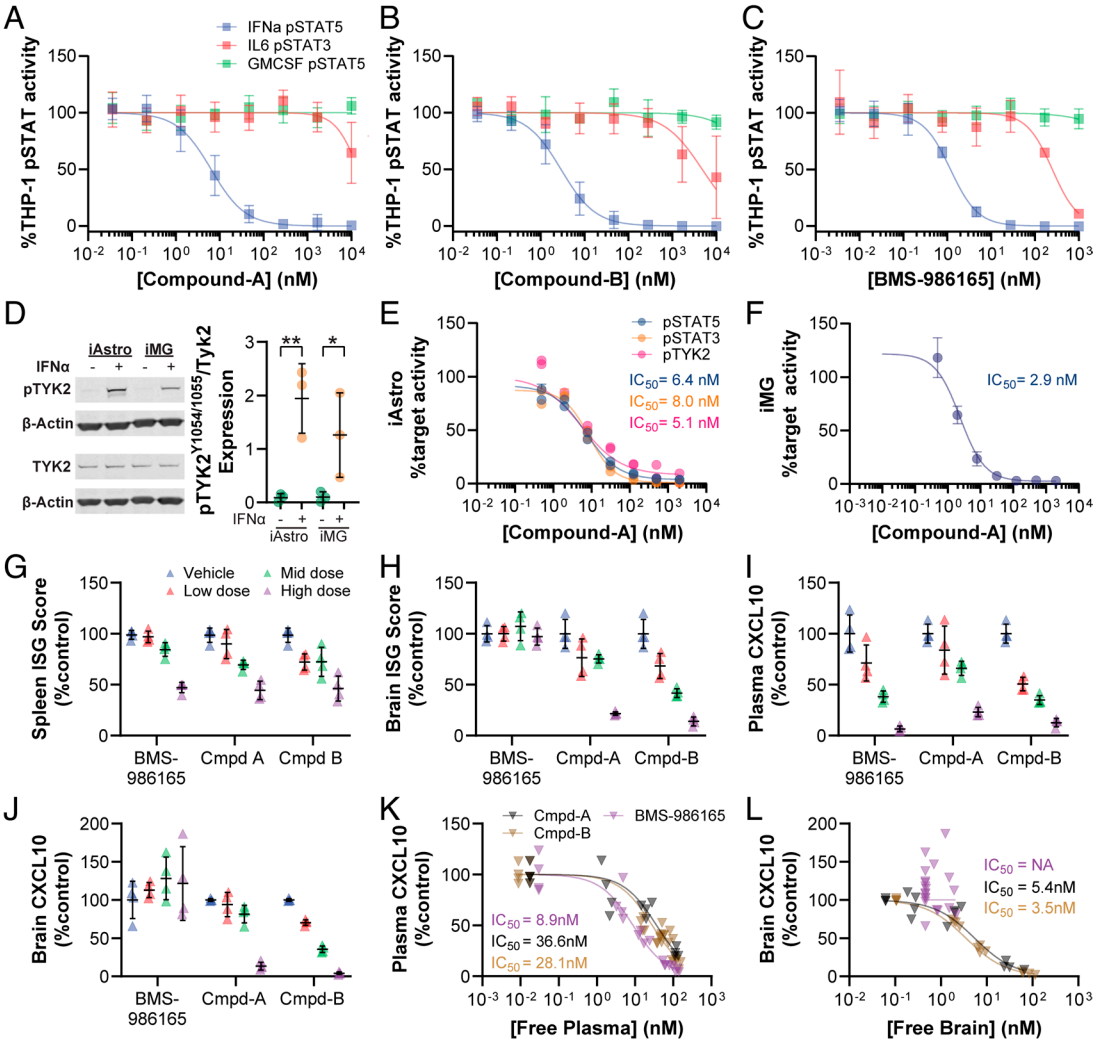

Fig. 1. Potent, selective, and CNS-penetrant TYK2 inhibitors attenuate IFNα- induced signaling in human iPSC-derived glia and rodent brain. Cellular potency and selectivity for (*A*) Cmpd-A, (*B*) Cmpd-B, and (*C*) BMS-986165 on TYK2, JAK1, and JAK2-dependent signaling pathways in THP-1 cells. n = 4 to 6. IFNα-induced phosphorylation of STAT5 shows TYK2 signaling, IL-6-induced phosphorylation of STAT3 shows JAK1 signaling and GM-CSF-induced phosphorylation of STAT5 shows JAK2 signaling. (*D*) Total and phosho-TYK2$^{Y1054/1055}$ immunoblot of from human iPSC-derived astrocyte (iAstro), and microglia (iMG) stimulated with IFNα. Cellular potency of Cmpd-A determined by ELISA against pSTAT3, pSTAT5, and pTYK2$^{Y1054/1055}$ in iAstro (*E*) and iMG (*F*) stimulated by IFNα. Data are presented as mean ± SD from three independent experiments. In vivo target engagement for Cmpd-A, Cmpd-B, and BMS-986165 in IFNα-induced C57BL/6 mice quantified by interferon-stimulated genes (ISG) mRNA expression in (*G*) spleen and (*H*) brain, and CXCL10 protein accumulation in (*I*) plasma and (*J*) brain. PK/PD relationship for each molecule was visualized by plotting CXCL10 levels against free drug concentrations in (*K*) plasma and (*L*) brain. CXCL10 value is represented as percent of vehicle control. Low = low dose group (0.3 mg/kg BMS-986165; 10 mg/kg Cmpd-A and Cmpd-B), Mid = mid dose group (1 mg/kg BMS-986165; 30 mg/kg Cmpd-A and Cmpd-B), High = high dose group (5 mg/kg BMS-986165; 100 mg/kg Cmpd-A and Cmpd-B). IC_{50} curves were fit using a nonlinear regression model weighted by $1/Y^2$ assuming normal pharmacology. Each dot represents an independent sample. ROUT test (Q = 1%) used to eliminate outliers. Bars represent mean ± SD. Statistical analysis was calculated using one-way ANOVA with Dunnett's multiple comparisons test.

Table 1. Cellular and in vivo properties of Compound-A, Compound-B and BMS-986165

Stimulus	Cell/tissue	End-point	Cmpd-A	Cmpd-B	BMS-986165
In vitro IC_{50} (nM)					
IFNα	THP-1	pSTAT5	6.4	2.9	1.2
IL-6	THP-1	pSTAT3	>10,000	4,793	250
GM-CSF	THP-1	pSTAT5	>10,000	>10,000	>1,000
IFNα	iAstrocyte	pTYK2	5.1	n/a	n/a
IFNα	iAstrocyte	pSTAT5	6.4	n/a	n/a
IFNα	iAstrocyte	pSTAT3	8.0	n/a	n/a
IFNα	iMicroglia	pSTAT5	2.9	n/a	n/a
IFNα	Whole blood	pSTAT1	n/a	2.1	1.1
IL-12	PBMC	pSTAT4	14.3	8.8	6.2
IL12/IL18	PBMC	IFNγ	98.9	47.2	19.8
In vivo IC_{50} (nM)					
IFNα	Plasma	CXCL10	36.6	28.1	8.9
IFNα	Brain	CXCL10	5.4	3.5	n/a
In vivo properties					
N/A	Plasma	PPB (%)	99.32%	99.19%	89.30%
N/A	Brain	BPB (%)	99.90%	99.76%	90.32%
N/A	Brain	Kp	0.78	0.49	0.026

iAstrocyte (iPSC-derived astrocytes); iMicroglia (iPSC-derived microglia); Plasma protein binding (PPB); Brain protein binding (BPB); Peripheral blood mononuclear cells (PBMC); Partition coefficient (Kp)

to BMS-986165, improved selectivity with lower potency toward IL-6-pSTAT3, and high selectivity with minimal potency against GM-CSF-pSTAT5. We also confirmed potency and selectivity biochemically, for both the kinase (JH1) and pseudokinase (JH2) domains of TYK2, JAK1, JAK2, and JAK3-(JH1 only). Like BMS-986165, Cmpd-A and B are selective for the TYK2 JH2 domain versus all other tested JAK domains (*SI Appendix*, Table S1). Additionally, we observed no activity against JAK JH1 domains at concentrations necessary to completely inhibit TYK2 activity via JH2 binding.

To evaluate the expression and function of TYK2 in CNS-resident cell types, we used human iAstrocytes and iPSC-derived microglia (iMicroglia). Phosphorylation at tyrosine 1054 (pY1054) is known to activate TYK2 catalytic activity and is thus a directly proximal surrogate suitable for monitoring TYK2 kinase activity (21). Expression of TYK2 and its phosphorylation in response to IFNα were confirmed in each cell type by western blot (Fig. 1*D*). The potency of Cmpd-A (IC_{50} of 5.1 nM) against TYK2 in iAstrocytes was determined by ELISA measuring the induction of pY1054 following treatment with IFNα (Fig. 1*E*). Downstream signaling through TYK2 was also inhibited with an IC_{50} of 6.4 nM for pSTAT5 and 8.0 nM for pSTAT3 (Fig. 1*E*). The IC_{50} of Cmpd-A in iMicroglia was 2.9 nM as measured by reduction of IFNα-induced pSTAT5 (Fig. 1*F*). Collectively, we find TYK2 signaling can be induced robustly in astrocytes and microglia by IFNα and inhibited by Cmpd-A.

Only Centrally Penetrant TYK2 Inhibitors Reduce Type I IFN Pathway Activity in the CNS. TYK2 is associated with the type I IFN receptor, which is ubiquitously expressed on most cell types and plays a crucial role in innate and adaptive immune responses. Binding of type I IFN to its receptor kicks off a cascade of phosphorylation events result in expression of interferon stimulated genes (ISGs, *SI Appendix*, Table S3) and other proinflammatory cytokines (22, 23). We employed a mouse model of acute IFN challenge and measured ISG signature and CXCL10 protein, to assess target engagement and the pharmacokinetic/pharmacodynamic (PK/PD) relationship of multiple TYK2 inhibitors. It is important to note, intraperitoneal (IP) injection of recombinant IFNα into the peripheral compartment induces robust activation of type I IFN pathway activity in peripheral and central compartments (Fig. 1). The expression and distribution of *Tyk2* in mouse CNS was confirmed and the expression patterns show *Tyk2* is expressed in microglia, astrocytes, and neurons through colocalization with *Aif2, Gfap*, and *Rbfox3* mRNA, respectively (*SI Appendix*, Fig. S1). Due to substantial differences in mouse PK and plasma binding properties (Table 1), BMS-986165 was administered at lower doses (0.3, 1, 5 mg/kg) than Cmpd-A and Cmpd-B (10, 30, 100 mg/kg) to achieve similar free-drug concentrations in the plasma across all molecules tested. Dose-dependent reduction of ISGs and C-X-C motif chemokine 10 (CXCL10) was observed in the spleen and plasma for all compounds tested (Fig. 1 *G–I*). The IC_{50} of BMS-986165 (8.9 nM) in plasma is slightly more potent than Cmpd-A and Cmpd-B (36.6 nM and 28.1 nM, respectively; Fig. 1*I*). In contrast, only cTYK2i Cmpd-A and Cmpd-B, reduced type I IFN pathway activity in the brain (Fig. 1 *J–K*). IC_{50}s of Cmpd-A and Cmpd-B are comparable in the brain (5.4 nM and 3.5 nM, respectively; Fig. 1*L*). The brain IC_{50} values were used to model and determine target coverage values and doses required for efficacy in the in vivo studies described below (*SI Appendix*, Table S2).

Central TYK2 Inhibition Required to Improve Clinical Score in the MOG_{35-55} EAE Mouse Model. Mice harboring a catalytically hypomorphic *Tyk2* allele (P1124A) and *Tyk2* KO mice are protected against EAE (10–12). However, the protection cannot be attributed to peripheral or central reduction of TYK2 activity in these models. To assess the impact of pTYK2i (BMS-986165) vs the cTYK2i (Cmpd-A) both compounds were delivered in a semitherapeutic paradigm in the murine MOG_{35-55} EAE model (24). Cmpd-A was dosed at 150 mg/kg/day to achieve unbound C_{ave} IC_{75} target coverage in the central compartment resulting in 23.4x IC_{50} target coverage in the periphery. To normalize peripheral impact of TYK2 inhibition of the two molecules BMS-986165 was dosed at 4 mg/kg/day providing unbound C_{ave} 27.4x IC_{50} target coverage in the periphery (*SI Appendix*, Table S2). Fig. 2*A* shows robust and dose-dependent reduction of clinical score in animals receiving the Cmpd-A, which was corroborated by lesser reduction of body weights (*SI Appendix*, Fig. S2*A*). The IC_{75} targeting dose (150 mg/kg/day) rescued clinical score by 84% overall while sub-IC_{50} targeting dose (60/mg/kg/day) resulted in a 63% reduction (*SI Appendix*, Table S2). BMS-986165 showed a slight but nonsignificant reduction of clinical score when compared to vehicle. Previous studies demonstrate protection against EAE in the TYK2 modified mouse models is particularly due to the impact on CNS-infiltrating $CD4^+$ T cells (10–12). Similarly, we demonstrate a dose-dependent reduction in the CNS-infiltrating population of $CD3^+/CD4^+$ T cells (Fig. 2*B*). The CNS-infiltrating T cell population reduction is associated with central IC_{50} target coverage (Fig. 2*C*). Dysregulation of ISGs has been demonstrated in EAE and human MS (25). ISG score in EAE brains was significantly reduced by Cmpd-A and reduction of T cell infiltrate correlates strongly with reduction of interferon signaling (Fig. 2 *D* and *E*). A confirmatory assessment of cTYK2i efficacy in MOG_{35-55} EAE model was performed with Cmpd-B. Again, the clinical score was reduced significantly by the semitherapeutic treatment of Cmpd-B along with reduction

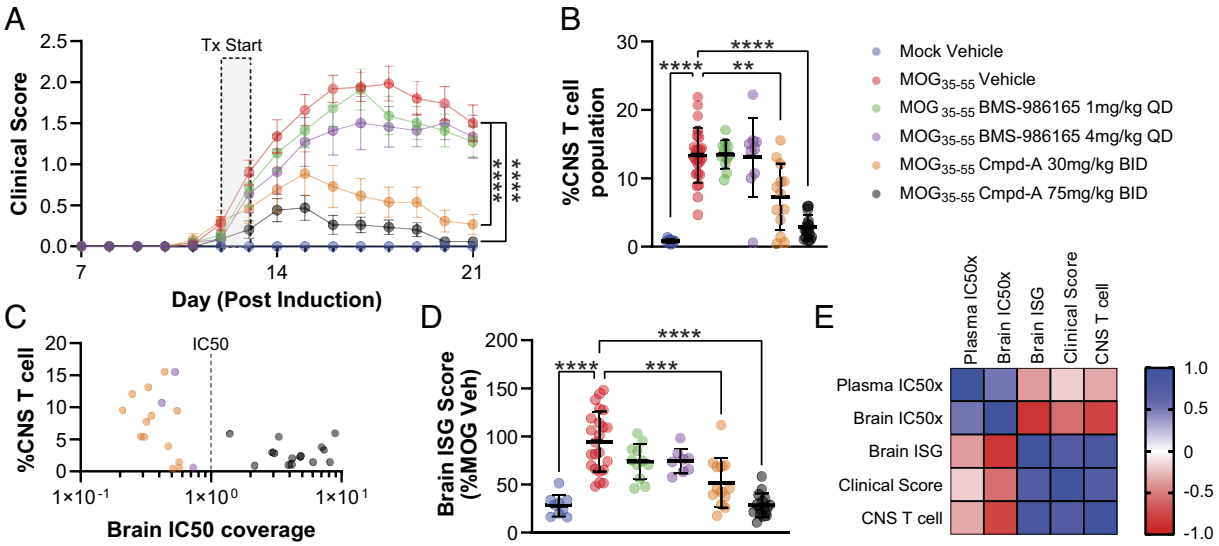

Fig. 2. Central TYK2 inhibition is protective by semitherapeutic delivery in the MOG_{35-55} EAE mouse model. (*A*) Clinical score for mock or MOG_{35-55} induced animals treated with vehicle, BMS-986165, or Cmpd-A, n = 9 to 24. Bars represent mean ± SEM and statistical analysis compares to cumulative clinical score of MOG_{35-55} EAE vehicle group. (*B*) CNS T cell population represented as % of total live cells following dissociation as determined by flow cytometry. (*C*) Correlations between CNS T cell population and brain IC_{50} coverage of tested compounds. (*D*) Brain ISG score. Bars represent mean ± SD and the data are representative of four independent experiments. Each dot represents an individual animal (*E*) Correlation heatmap comparing target coverage (IC_{50}x), brain ISG, clinical score, and CNS T cell population. Statistical analysis compares to MOG EAE vehicle group using one-way ANOVA with Dunnett's multiple comparisons test, Brown–Forsythe, or Welch ANOVA with Dunnett's T3 multiple comparison test based on data distribution.

of CNS- infiltrating effector T cells (*SI Appendix*, Fig. S3 *A* and *B*). Pharmacologically, we recapitulated previous findings from Gorman et al. (12) and Dendrou et al. (10) showing TYK2 signaling impairment results in reduced proportion of Th_1 and Th_{17} cells infiltrating the CNS (*SI Appendix*, Fig. S3 *C–E*). The selective impact of cTYK2i on clinical score, T cell infiltration, and IFN pathway activity emphasizes the importance of targeting neuroinflammation from the "inside out" in EAE.

cTYK2i Reverses Clinical Score in MOG_{1-125} EAE Despite Minimal Impact on Circulating MOG IgG. EAE induction by different myelin antigens results in unique pathologies that are segregated by T cell and B cell driven pathologies. In the MOG_{1-125} model, B cells drive endogenous antibody-mediated demyelination is not necessary for MOG-induced EAE but contributes to severity (24, 26). To assess the impact of TYK2 inhibition on B cell–driven pathologies involved in EAE the cTYK2i Cmpd-B and pTYK2i BMS-986165 were delivered to animals immunized with MOG_{1-125} in an exposure-matched full-therapeutic dosing regimen. The cTYK2i was able to reverse clinical scores when treatment was initiated after presentation of clinical symptoms and was more impactful than pTYK2i on reducing clinical score (Fig. 3*A*). Confirming clinical remission, cTYK2i treatment normalized distance traveled in open field when compared to mock animals (Fig. 3*B*). When examining peripheral cell infiltrate in the CNS only the high dose of Cmpd-B (60 mg/kg/day, > C_{ave} IC_{75}) showed a significant reduction of $CD3^+/CD4^+$ T cells (Fig. 3*C*) and reduced proportion of Th17 (*SI Appendix*, Fig. S4). However, B cells ($CD3^-/B220^+$) were reduced by ~40% in all treatment groups (Fig. 3*D*), suggesting reduction was largely a result of peripheral TYK2 inhibition. Additionally, the level of plasma IgG directed against the human MOG_{1-125} antigen was unaffected by treatment (Fig. 3*F*). Total circulating T cells and B cells were largely unimpacted by TYK2i with a trend toward reduction (*SI Appendix*, Fig. S4 *D* and *E*). Again, central IC_{50} target coverage correlated strongly with clinical score, brain ISG score and T cell infiltrate but not B cell infiltrate or MOG IgG (Fig. 3*E*). Clear rescue of clinical deficits by the cTYK2i in absence of robust impact on circulating MOG^+ IgG highlights the importance of targeting T cell biology to significantly impact EAE as a preclinical model of MS.

Microglial Activation Is Impaired by cTYK2i in EAE. Microglia and astrocyte activation are hallmarks and key drivers of pathology in neuroinflammation and EAE (26–28). To identify impacts of cTYK2i on demyelination and glial cell activation, the spinal cords of a subset of animals (n = 3/group/ region, balanced by clinical score) were assessed for astrogliosis and microgliosis by immunohistochemistry (IHC). Increased $GFAP^+$ and $Iba1^+$ cell populations were evident in MOG-immunized spinal cords, indicative of increased activated astrocyte and microglial populations. Cmpd-B and BMS-986165 did not have a clear impact on the reactive astrocyte population (Fig. 4*A*) based on $GFAP^+$ pixel area. However, there was a significant reduction in the $Iba1^+$ cell population in animals that received Cmpd-B, highlighted by reduced regions of focal infiltrate (Fig. 4*B*). Areas of demyelination, coinciding with microglial infiltrate, were visualized by MBP immunostaining counterstained with neutral red (NR) (Fig. 4*C*, white arrows). The cTYK2i treatment significantly reduced the area of demyelination in the spinal cord (Fig. 4*C*). Overall, IHC data could suggest selective impact of TYK2 inhibition on microgliosis however, further investigation into markers of reactive astrocyte and microglial populations is warranted. This finding suggests central TYK2 inhibition is key to reduction of neuroinflammation from the "inside out" whereby TYK2 inhibition in microglia may be sufficient to reduce proliferation and subsequent demyelination.

cTYK2 Inhibition Abates Type I Interferon and NF-κB Signaling to Extinguish Neuroinflammatory Program. NF-κB pathway activation has been identified in multiple cell types in or near active CNS lesions in postmortem brain tissue from MS patients (29–32), and deficiency in some NF-κB pathway-associated proteins is protective against EAE (33, 34). Evidence exists that noncanonical NF-κB pathway activation plays a role in the production of type I IFNs (35, 36). Given the known crosstalk between IFN and NF-κB pathways (37), our evidence of

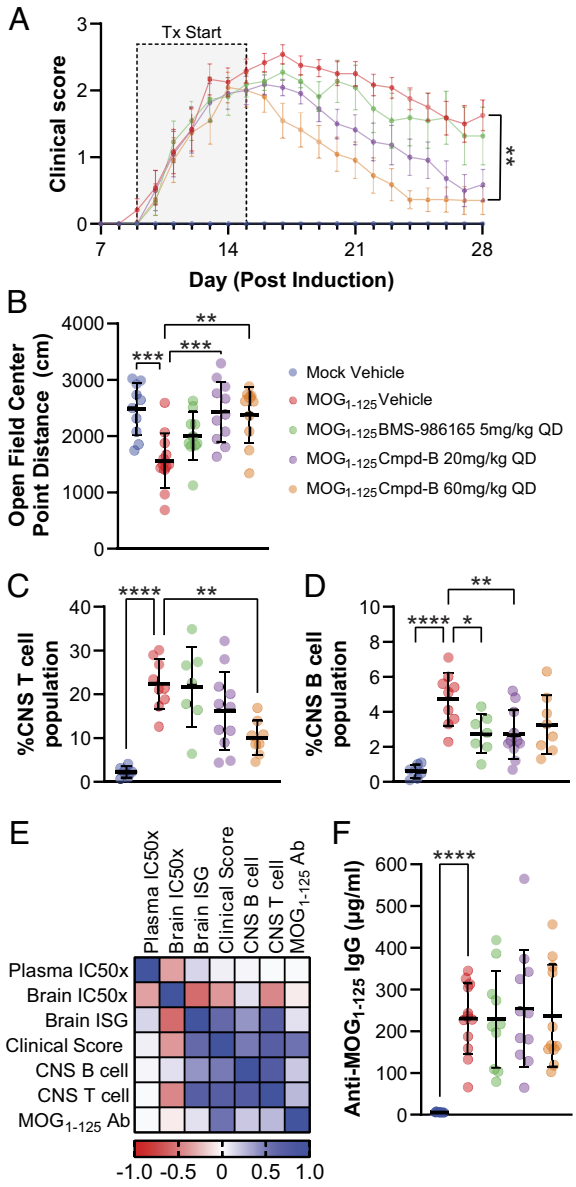

Fig. 3. Central TYK2 inhibition is protective by therapeutic delivery in the MOG_{1-125} EAE mouse model. (*A*) Clinical score was recorded daily for mock or MOG_{1-125} induced animals treated with vehicle, BMS-986165, or Cmpd-B. Bars represent mean ± SEM from two independent experiments and statistical analysis compares to cumulative clinical score of MOG_{1-125} EAE vehicle group, n = 10 to 11. (*B*) Endpoint open field motor test. (*C*) CNS T cell and (*D*) B cell population are represented as % of total live cells. Bars represent mean ± SD and the data are representative of two independent experiments (*E*) Correlation heatmap comparing target coverage, brain ISG, clinical score, and CNS T or B cell population. (*F*) Plasma levels of anti-MOG_{1-125} IgG. Bars represent mean ± SD. Each dot represents an independent animal. Statistical analysis compares MOG EAE vehicle groups to all other groups using one-way ANOVA with Dunnett's multiple comparisons test.

IFN pathway activity in EAE (Fig. 2*D*), and the effectiveness of cTYK2i in protecting against EAE severity (Figs. 2 and 3), we aimed to investigate the impact of TYK2 inhibition on NF-κB and IFN pathways more broadly. To this end, we ran a targeted gene expression analysis on whole brain samples from MOG_{35-55} and MOG_{1-125} EAE mice treated with cTYK2i and pTYK2i using curated Taqman Array Cards. In the MOG_{35-55} model, 66/72 genes dysregulated in response to MOG_{35-55} induction were significantly rescued by cTYK2i, not pTYK2i. In the MOG_{1-125} model, 29/54 genes dysregulated in response to MOG_{1-125} induction were significantly rescued by cTYK2i, not pTYK2i (Fig. 5 *A–D* and *SI Appendix*, Tables S4-S9). Among the list of genes preferentially rescued by cTYK2i are several members of TLR and interferon response factor (IRF) families, regulators of canonical and noncanonical NF-κB pathway activity, IFN-inducible antiviral genes, class I and II cytokine signaling receptors, and several factors involved in autocrine and paracrine inflammatory signaling. The observation that most genes dysregulated in EAE mouse brains were preferentially affected by a centrally penetrant TYK2i (Fig. 5 *A–D*) supports the hypothesis that TYK2 is involved in driving a CNS-specific inflammatory program in EAE.

Neuroinflammatory Biomarkers Dampened by cTYKi in EAE. In alignment with previous meta-analyses highlighting the emergence of cytokines and chemokines as robust biomarkers in MS patient blood and CSF (38, 39), we evaluated proinflammatory markers in the context of TYK2 inhibition. Spinal cord samples collected from MOG_{35-55} or MOG_{1-125} EAE mice were analyzed for cytokine and chemokine levels. Significant elevations in cytokines, including IL-6 and IL-1b, and chemokines, such as CXCL10, IL-16, CCL2, CCL3, CCL4, and CXCL13 were detected in vehicle-treated MOG-immunized animals when compared to mock (Fig. 5 *E–G* and *SI Appendix*, Figs. S3*G* and S5). (Fig. 5*H* and *SI Appendix*, Fig. S3*H*). Notably, the administration BMS-986165, Cmpd-A, or Cmpd-B lowered the levels of proinflammatory cytokines IL-6 and IL-1β in the spinal cord tissue from EAE mice in a dose-dependent manner (*SI Appendix*, Figs. S3*G* and 5 *D* and *F*). However, chemokines exhibited a stronger correlation with CNS-infiltrating $CD4^+$ T cell counts and EAE severity than cytokines (Fig. 5*H*). The results showed a positive correlation between CCL3 with the clinical severity of EAE ($r = 0.80$, $P < 0.0001$), and lymphocyte infiltration ($r = 0.82$, $P < 0.0001$) in the spinal cord of EAE mice, while IL-1β shows $r = 0.24$, $P < 0.05$ and $r = 0.4$, $P < 0.001$). A subset of analytes, including IL-2, CXCL10, IL-16, CCL3, CCL4, and CXCL13 responded exclusively to cTYK2i treatment but not to BMS-986165, suggesting a selective effect of cTYK2i (Fig. 5 *E–H* and *SI Appendix*, Fig. S5 *A–C* and *E*). The IL-23/Th_{17} axis has been demonstrated to play an essential role for EAE development (40). Consistent with previous studies, our data demonstrated the MOG-induced elevation of IL-12/IL-23p40 and IL-17A levels in the spinal cord, while Cmpd-B treatment rescues the levels to 24% or 10% of control, respectively (*SI Appendix*, Fig. S5 *G* and *H*). Cmpd-B also significantly reduced the neuroinflammation biomarkers in MOG_{1-125} EAE model, while administration of BMS-986165 only slightly ameliorated the inflammation within the spinal cord (Fig. 5 *E–H*). Finally, neuroinflammatory analytes show better correlation with $CD4^+$ T cell than B cell in the CNS (Fig. 5*H* and *SI Appendix*, Fig. S3*H*). This finding confirms a more prominent impact on pathogenic $CD4^+$ T cells response in the TYK2-mediated neuroinflammatory pathway.

cTYK2i Is Protective in the MS Model Driven by Pathogenic Recombinant Antibodies (rAb) Derived from B Lymphocytes in PPMS Patient CSF. A recent study of Wong et. al. (41) describes the unique capacity of PPMS CSF to induce motor disability and spinal cord pathology in a translational MS mouse model (Fig. 6*A*). Moreover, the delivery of rAb derived from sequencing B lymphocytes present in PPMS CSF recapitulates PPMS pathology. Prophylactic treatment with Cmpd-B (60 mg/kg/day) in this model provided protective effects on motor deficit score and grip strength (Fig. 6 *B* and *C*). The model has a rapid onset (1 to 3 d) and short duration and therefore requires prophylactic dosage to assess impact of treatment. Like findings from the MOG_{1-125} model, assessment of $GFAP^+$ astrocyte population in spinal cords did not show a significant decrease with cTYK2i treatment while $Iba1^+$ microglia were reduced in the cTYK2i-treated animals (Fig. 6

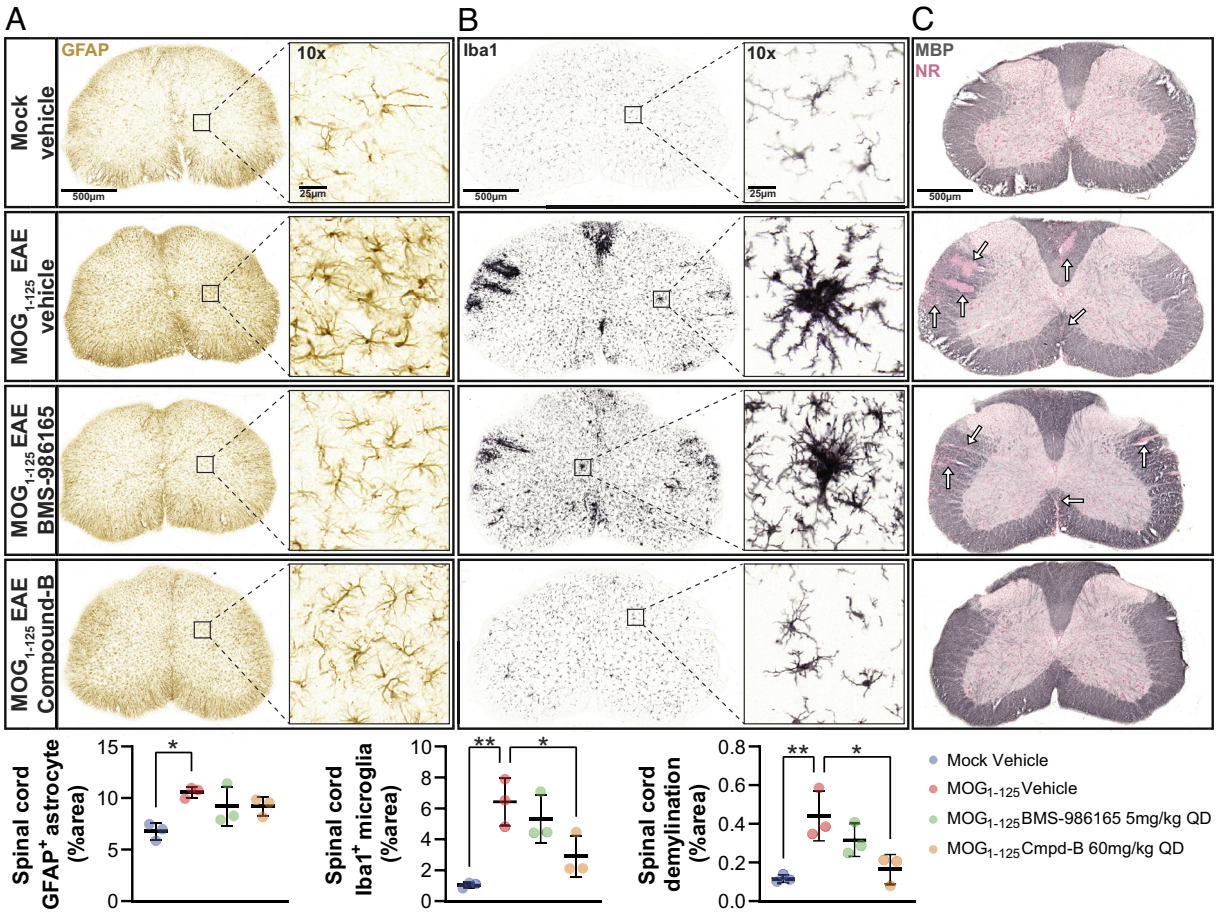

Fig. 4. Central TYK2 inhibition reduces demyelination and gliosis in the MOG_{1-125} EAE mouse model. Representative brightfield images and quantifications for cervical spinal cord coronal sections immunohistochemically stained for (*A*) GFAP, (*B*) Iba1 and (*C*) MBP in mock or MOG_{1-125} induced animals treated with vehicle, BMS-986165, or Cmpd-A. MBP stain is counterstained with Neutral Red (NR). Percent area measurements are relative to total tissue area per ample. Bars represent mean ± SD from two independent experiments. Each dot represents an independent animal. Statistical analysis compares MOG EAE vehicle groups to all other groups using one-way ANOVA with Dunnett's multiple comparisons test.

D–*E*). SMI-32 signal was also significantly reduced by cTYK2i indicating a reduction in neuronal damage or degeneration within the spinal cord (Fig. 6*F*). Interestingly, the model does not show evidence of specific antigen recognition within the spinal cord and the interaction of the human rAb with the F_c receptors on the surface of glial population is presumably the driver of pathology (41). This suggests reduction of neuroimmune activation by a cTYK2i can occur without the antigen-presenting component or cognate T cell–microglial interactions known to drive EAE (42) and possibly Relapsing Remitting MS (RRMS)/PPMS.

Neurodegeneration Marker NfL Reduced in CSF and Plasma by cTYK2 Inhibitor in EAE. NfL concentrations in CSF and peripheral blood compartments were established as reliable surrogates of neuronal injury across a spectrum of neurodegenerative pathologies (43). Within the context of MS, longitudinal NfL assessments have prognostic significance, delineating disease trajectory in relapsing-remitting as well as progressive subtypes, while concurrently tracking therapeutic efficacy and clinical exacerbations (44). In an experimental model of MS employing EAE rats, we quantified NfL levels in plasma (pNfL) and CSF (cNfL). A marked increase in NfL was observed in the cohort challenged with MBP peptide MBP_{69-88} compared to the control group, with a significant attenuation upon treatment with Cmpd-A (Fig. 7*B*). This therapeutic modulation of cNfL was mirrored in pNfL concentrations, affirming the translational utility of blood-based surrogate biomarkers (Fig. 7*D*). Correlation analyses substantiated a robust association between cNfL and clinical severity as well as pNfL ($r = 0.83$, $P < 0.001$; and $r = 0.63$, $P < 0.001$, respectively) (Fig. 7 *C* and *E*). Additionally, pNfL levels were reduced by Cmpd-B treatment in the MOG_{1-125} EAE model (*SI Appendix*, Fig. S3 *I* and *J*). Collectively, these findings demonstrate inhibiting central TYK2 activity reduces neuroinflammation, thereby imparting neuroprotection in demyelinating diseases.

Tyk2 Modifies IRRA Function. IRRAs, a subset of reactive astrocytes induced by type I IFN/TNF-α/IL-1α/C1q, were identified around perivascular, periventricular, subpial spaces in mice following LPS-induced inflammation. IRRA populations have also been found in the acute phase of EAE with a decrease during remission and correlate with disease severity and progression (45). To investigate the role of Tyk2 in astrocyte activation, we treated iAstrocytes with TNF-α, IL-1α, and C1q (TIC) to induce an A1-like phenotype, or combined TIC with 100 ng/ml of human IFNβ to induce an IRRA-like phenotype for 24- and 48-h (Fig. 8 and *SI Appendix*, Fig. S7). A1-like and IRRA-like astrocytes exhibited a hypertrophic phenotype, characterized by increased cellular compaction and enhanced arborization (*SI Appendix*, Fig. S6*A*). Inhibition of TYK2 activity resulted in a dose-dependent suppression of hypertrophic phenotype, indicating its role in regulating astrocytic morphological changes (*SI Appendix*, Fig. S6*C*). To verify cell-type identity after treatment, we

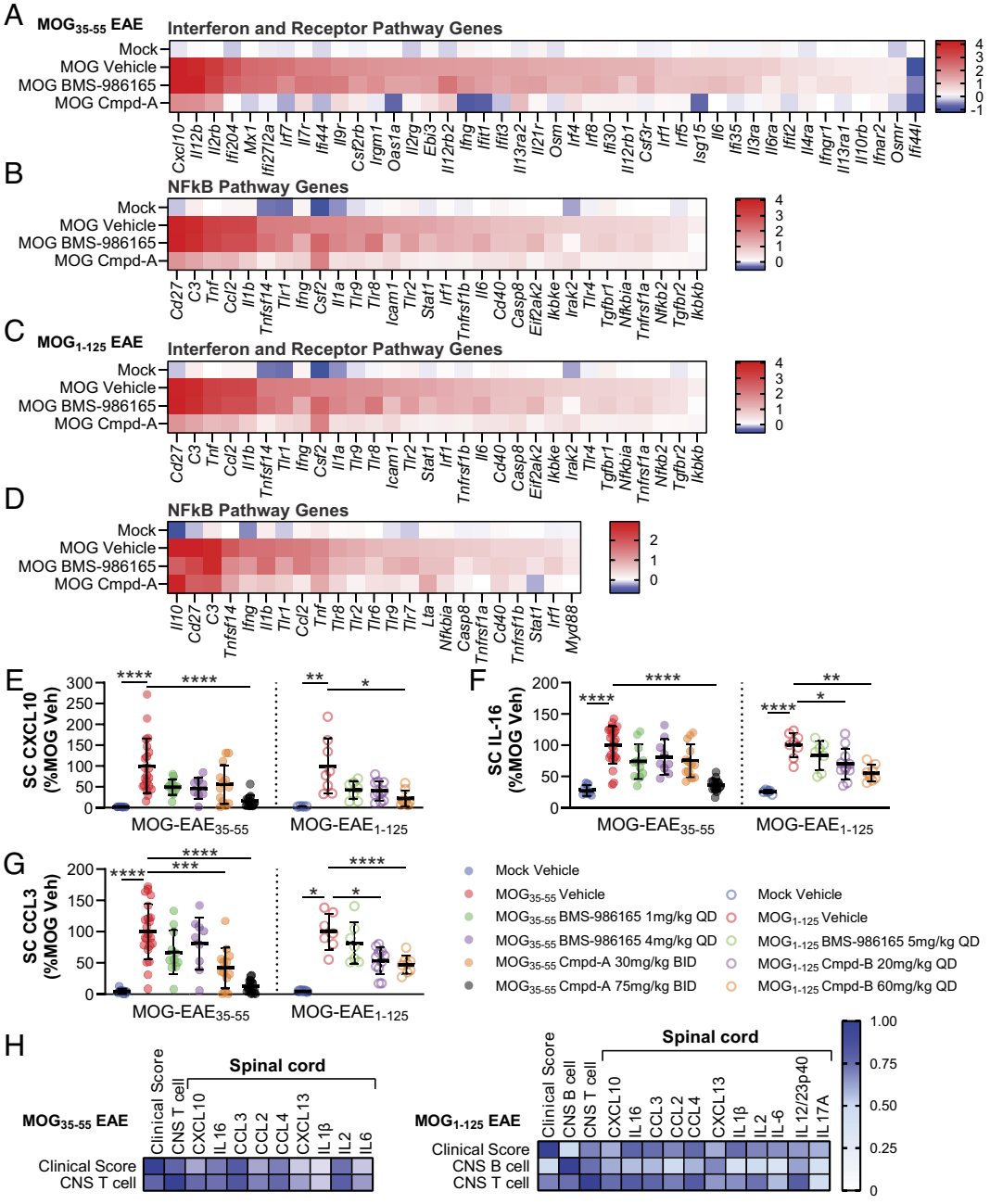

Fig. 5. Central TYK2 inhibition attenuates transcriptional inflammatory program and biomarker expression in EAE mouse models. MOG_{35-55} (*A*) IFN and (*B*) NF-κB mediated whole brain mRNA expression and, MOG_{1-125} (*C*) IFN and (*D*) NF-κB mediated whole brain mRNA expression represented as heat map of median Log2 fold change (Log2FC) relative to Mock vehicle group, n = 5 to 24. The relative levels of (*E*) CXCL10, (*F*) IL-16, and (*G*) CCL3 in the spinal cord tissue from Mock, MOG EAE induced animals treated with vehicle, BMS-986165, Cmpd-A, or Cmpd-B. Results are reported as relative levels to the EAE vehicle group per experiment and represent mean ± SD. Each dot represents an independent animal. (*H*) Cytokine and chemokine correlation to clinical score and CNS T cell population in MOG EAE models. Statistical analysis compares to MOG EAE vehicle group using one-way ANOVA with Dunnett's multiple comparisons test, Brown–Forsythe, and Welch ANOVA with Dunnett's T3 multiple comparison test or Kruskal–Wallis with Dunn's multiple comparison based on data distribution.

measured expression of known markers of A1-like cells (Reactive Score), IRRA-like cells (Reactive and Interferon Scores), and type I IFN pathway activity (Interferon Score) in each iPSC-derived astrocyte subtype (*SI Appendix*, Table S3) (45–47). All genes tested were upregulated in both TIC- and TIC+IFNβ-treated cells, but cells treated with type I IFN exhibited greater changes in gene expression, as demonstrated by the Comprehensive Score (Reactive and Interferon Scores; Fig. 8*A*). To understand whether the elevated Comprehensive Score in TIC+IFNβ-treated cells is driven by type I IFN alone, we generated additional scores specific to interferon pathway activity and astrocyte reactivity (Interferon Score). As expected, cells treated with TIC+IFNβ have a more robust Interferon Score compared to cells treated with TIC alone (Fig. 8*B*). We also observed a more robust Reactive Score in cells treated with TIC+IFNβ compared to TIC alone (Fig. 8*C*), which suggests addition of type I IFN exacerbates overall reactivity in this cell type. We did not observe a TYK2i-dependent reduction in any score for iAstrocytes treated with TIC alone. However, we observed dose-dependent reduction of all scores in response to TYK2i in cells treated with TIC+IFNβ (Fig. 8 *A*–*C*).

To ask whether astrocytes were able to mount a functional immune response to TIC or TIC+IFNβ, we examined the secretion profiles of the astrocyte-conditioned media (ACM) at 24- (*SI Appendix*, Fig. S7) and 48-h poststimulation (Fig. 8). Stimulation with TIC or TIC+IFNβ increased the release of chemokines and cytokines (Fig. 8*D* and *SI Appendix*, Fig. S7*D*). Compared to TIC, TIC+IFNβ further increased the release of proinflammatory factors (IL-6: TIC + IFNβ 1,653 ± 82 pg/ml vs. TIC 449 ± 83 pg/ml, $P < 0.01$; CCL3: TIC + IFNβ 2,070 ± 151 pg/ml vs. TIC 275 ± 25 pg/ml, $P < 0.0001$; CXCL10: TIC + IFNβ 1,610 ± 638 pg/ml vs. TIC 140 ± 31 pg/ml, $P < 0.0001$) (Fig. 8*D* and *SI Appendix*, Fig. S7*D*). Treatment with Cmpd-A dose-dependently decreased the levels of CCL3, CCL4, CXCL10, and IL-6 in IRRA-like cells, while selectively

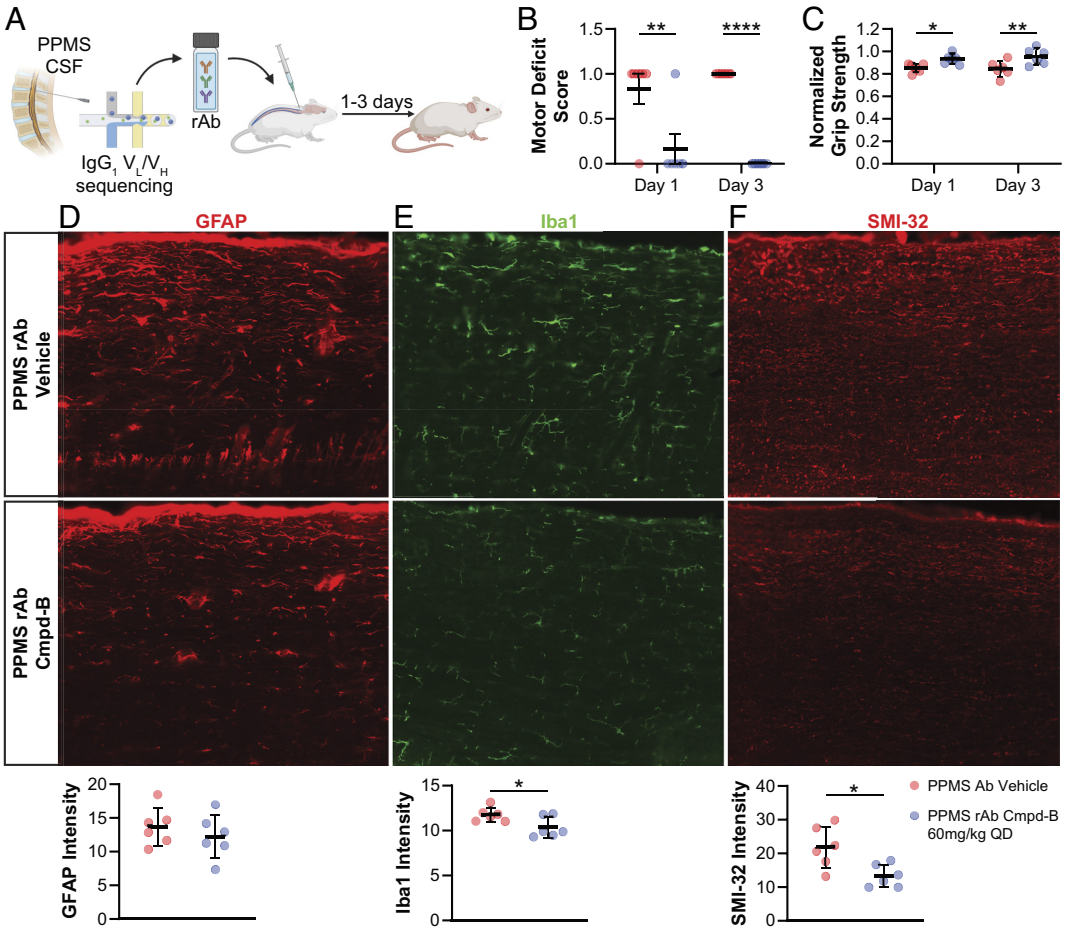

Fig. 6. Pathogenic rAb derived mouse model of PPMS rescued by prophylactic central TYK inhibition. (*A*) Schematic summarizing method of disease induction by administration of rAb derived from CSF B cells of PPMS patient. (*B*) Motor deficit score reported on days 1 and 3. Bars represent mean ± SEM. Each dot represents an independent animal (n = 6). (*C*) Normalized grip strength reported on days 1 and 3. Representative images and quantification for spinal cord (*D*) GFAP, (*E*) Iba1, and (*F*) SMI-32 staining. Bars represent mean ± SD. Each dot represents an independent animal. Statistical analysis was calculated using two-way ANOVA or unpaired two-tailed *t* test.

attenuating CXCL10 secretion in A1 (*SI Appendix*, Fig. S7 *B–G* and Fig. 8 *E–J*). Additionally, we observed upregulation of YKL-40, a glycoprotein used as a neuroinflammatory marker, in both astrocyte populations with higher levels detected in IRRA-like astrocytes (Fig. 8*D*). Inhibition of TYK2 activity blocked the elevation of YKL-40 in IRRA-like but not in A1-like cells (Fig. 8*J*). These findings suggest TYK2 plays a crucial role in regulating the reactivity and immune response function of IRRA-like cells, highlighting its potential as a therapeutic target in neurodegenerative diseases associated with astrocyte reactivity.

Discussion

Targeting CNS inflammatory pathways from the inside out is an emerging strategy to extinguish smoldering neuroinflammation (14, 15). The data presented establish TYK2 as a key neuroimmune modulator capable of regulating inflammatory insults within the central compartment in autoimmune disease (*SI Appendix*, Fig. S9). We demonstrated IFNα-induced TYK2 signaling pathway is intact within glial cells and selectively inhibited by our compounds. We show that peripheral disruption of TYK2-directed signaling pathways alone is insufficient to prevent pathogenesis and TYK2 inhibition from within the CNS is necessary for protection against antigen-mediated EAE. Interestingly, genetic ablation of the IL-12 and IL-23 pathway, drivers of T cell development, has an inconsistent impact on EAE whereby *Il12p35*$^{-/-}$ mice are hyperinflammed and *Il23p19*$^{-/-}$ mice are protected from EAE (48, 49). However, genetic ablation of the common p40 subunit (*Il12p40*$^{-/-}$), results in concomitant disruption of IL-12 and IL-23 signaling and protection against EAE (50). Accordingly, TYK2 plays a direct role in signal propagation from each of these cytokines and inhibition phenocopies the *Il12p40*$^{-/-}$ EAE mice. Further EAE experiments in tissue-specific KO strains may clarify the impact TYK2 inhibition on IL-12 vs IL-23 pathways in EAE. Our findings show cTYK2 inhibition leads to dampened chemoattractant signals (CCL2, CCL3, CCL4) emanating from the CNS (Fig. 5, *SI Appendix*, Fig. S5) thereby blunting the infiltration of myeloid antigen-presenting cells that help shape T cell immunity (51). Additionally, cTYK2i may disrupt cognate microglial-T cell interaction in the CNS that regulates balance of effector T cell and regulatory T cell populations in EAE (42). While we did not demonstrate an impact of cTYK2i on astrocyte populations by GFAP in EAE spinal cords, it is possible that A1 populations were established prior to treatment and resistant to changes in GFAP density or morphology. This hypothesis is supported by the impact of TYK2i on iPSC-derived astrocytes where inhibition had a robust impact on IRRA populations but minimal effect on A1-like populations (Fig. 8).

The efficacy of cTYK2i in the PPMS rAb mouse model highlights the role of TYK2 in mediating inflammatory signals via glial cells as the model relies on an antibody-based insult within the CNS. The *Tyk2* protective allele does not shield mice from autoantibody production and disease progression in two separate lupus models even though GWAS has linked this variant to protection from SLE (12). Consistent with this, we did not observe TYK2i impact on autoantibody production in MOG$_{1\text{-}125}$ EAE model.

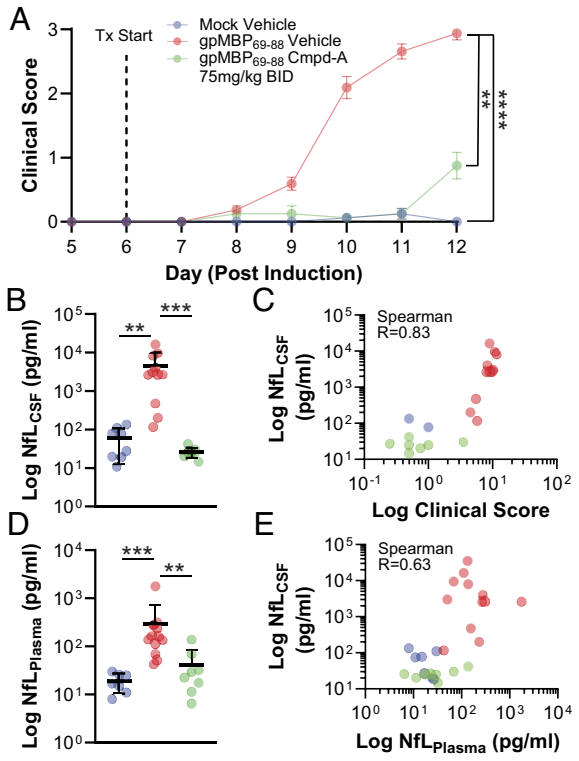

Fig. 7. NfL Biomarker correlates with disease severity in $gpMBP_{69-88}$ EAE rat model. (*A*) Clinical score was recorded daily for mock or MBP EAE induced animals treated with vehicle, BMSf-986165, or Cmpd-A, n = 8 to 16. Bars represent mean ± SEM and statistical analysis compares to cumulative clinical score of $gpMBP_{69-88}$ EAE vehicle group. (*B*) cNfL quantification and (*C*) correlation to clinical score. (*D*) pNfL quantification and (*E*) correlation to cNfL. Bars represent mean ± SD from two independent experiments. Each dot represents an independent animal. Statistical analysis compares to $gpMBP_{69-88}$ EAE vehicle group using the Kruskal–Wallis test with Dunn's multiple comparisons test.

This suggests unique mechanisms are at play within the central compartment for TYK2-mediated response to antibody-dependent inflammation (ADI) through Fc receptor families (52).

Among genes regulated by central TYK2i in EAE are multiple members of the TLR, IRF, NF-κB, interferon-induced antiviral response, and cytokine receptor families (Fig. 5 and *SI Appendix*, Tables S4–S7). TLRs signal through NF-κB and IRF transcription factors to drive expression of proinflammatory cytokines and type I IFNs, respectively. The elevated CNS expression of IRF and antiviral genes in EAE, likely driven by cellular damage and subsequent type I IFN pathway activation, may drive a positive feedback loop exacerbating proinflammatory CNS environment (53, 54). Our gene expression, T cell infiltration, and cytokine and chemokine data, suggest cTYK2i disrupts this positive feedback loop of inflammatory signaling in the CNS. The transcriptional factor NF-κB as a master regulator of immune response has been shown to be activated in multiple CNS cell types in MS patients and EAE (32). Similar to the cTYK2i data presented here, conditional knockout of NF-κB inducing kinase (NIK) in microglia limits EAE progression and has been shown to be essential for T cell recruitment to the CNS (28).

The cytokine and chemokine milieu orchestrates a balance of neuroinflammation and neuroprotection and dysregulation is often associated with disease. IL-16 is a chemotactic substance essential for promoting chronic inflammation driven by $CD4^+$ Th_1 cells with increases observed in active CNS lesions and biofluids of MS patients and EAE animals (55–58). Induction of CCL3 and CXCL10 in EAE aligns with known MS biology and highlights the interplay of infiltrating T cells with CNS-resident glia in pathogenesis. Both chemokines, signaling through C-C chemokine receptor 5 (CCR5) and CXC-chemokine receptor 3 (CXCR3) respectively, are known to be elevated in CSF and active lesions of MS patients. Circulating numbers of $CCR5^+/CXCR3^+$ T cells are also reported to be increased in progressive MS along with $CXCR3^+$ T cells in RRMS (59, 60). Dampening of glial IL-16, CCL3, and CXCL10 expression by cTYK2i is likely involved in the reduction of T cell numbers, altered inflammatory milieu, and improved clinical outcomes we see in multiple EAE models.

Reactive astrocytes are shown to contribute to the pathogenesis of several neurodegenerative diseases, including Alzheimer's Disease and MS by releasing proinflammatory cytokines and chemokines, which contribute to neurotoxic effects and exacerbate the progression of neurodegenerative diseases (61). Astrocyte reactivity is highly heterogenous and influenced by insult, which results in unique reactive subsets (45, 62). Hasel et al. demonstrated IRRA marker genes are enriched in astrocytes across various neurodegenerative models, including EAE, the 5xFAD model of Alzheimer's disease. Notably, astrocytic response to type I interferons has also been observed in CNS lesions from MS patients. In these brain samples, $GFAP^+$ astrocytes showed enrichment for pSTAT1 and MX1, indicating a potential involvement of IRRAs in modulating inflammation in multiple sclerosis. Despite the detection of IRRAs in diverse pathological contexts, their precise functional roles in these scenarios remain unclear. Our investigations suggest IRRA-like cell populations are more proinflammatory than A1 populations based on gene expression signature and secretion profile. TYK2 is involved in regulating the IRRA-like but not the A1 astrocyte reactivity and chemokine release (Fig. 8 and *SI Appendix*, Fig. S7). Whether TYK2 regulates other functions in the definition of reactive astrocyte subtypes needs to be explored further.

The capacity of TYK2 inhibition to rescue MS pathology and inhibit type I IFN signaling appears to be incongruous with the therapeutic efficacy of IFNβ treatment for some patients. However, the response to IFNβ is heterogenous, which includes up to 40% of patients that do not respond or respond poorly to treatment as defined by relapse rate or disability progression (63, 64). The underlying mechanism behind the lack of therapeutic effect of IFNβ in some patients may be due to differential cytokine and chemokine production in responders (65, 66). It has also been observed that IFNβ treatment can exacerbate Th17-induced EAE and synergize with IL-23 to drive the inflammatory program, which is in concordance with evidence that type I IFNs worsen disease in patients with high serum IL-17F and neuromyelitis optica (67, 68). The therapeutic benefit of IFNβ is a confound in the field. Although we would expect TYK2 inhibition to be counter to the IFNβ therapeutic effects, genetic data in humans (protective hypomorphic TYK2 P1104A) and our EAE data suggest otherwise.

Collectively, we have presented data that elucidate a coherent mechanism for the role of TYK2 in regulation of neuroinflammation. We demonstrated central inhibition of TYK2 is required for modulation of EAE pathophysiology. Type I IFN-induced TYK2 signaling pathway is functional within glial cells and selective inhibition can result in a pleiotropic impact that extinguishes the neuroinflammatory program at the embers/source. The mechanisms presented here strengthen the strategy for targeting central TYK2 for treatment of MS.

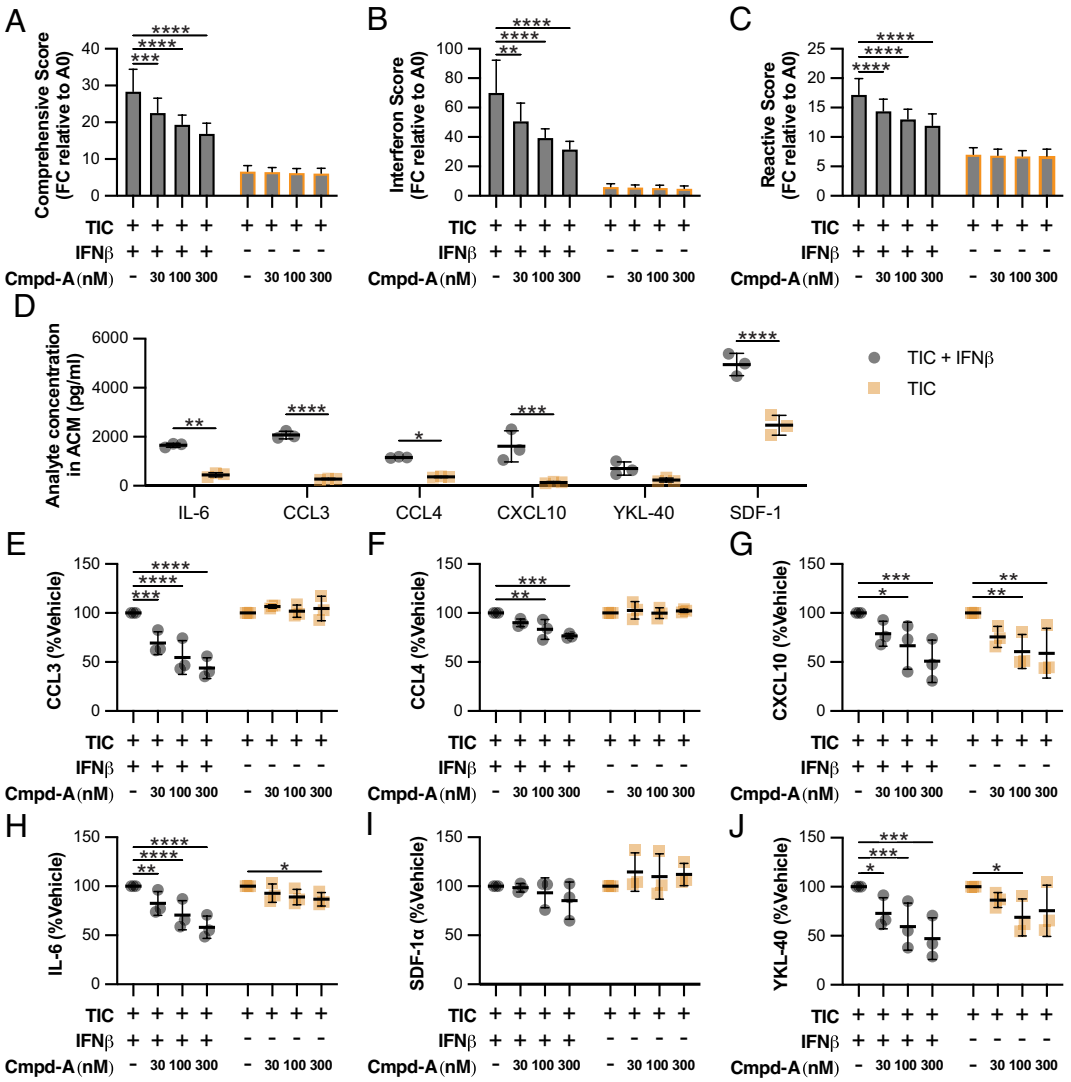

Fig. 8. Differential effects of TYK2 inhibition on iPSC-derived reactive astrocyte models. (*A*) Comprehensive, (*B*) Interferon, and (*C*) Reactive gene expression scores from two iPSC-derived reactive astrocyte models treated with TYK2 inhibitor for 48 h. Scores represent the geometric mean of fold change across all genes tested relative to unstimulated cells. (*D*) Comparison of secreted cytokines in astrocyte-conditioned medium across iPSC-derived astrocyte models. Relative levels of (*E*) CCL3, (*F*) CCL4, (*G*) CXCL10, (*H*) IL-6, (*I*) SDF-1α, and (*J*) YKL-40, with DMSO or Cmpd-A at poststimulated 48 h. Each dot represents an independent sample. Bars represent ± SD from three independent experiments and statistical significance was calculated using two-way ANOVA.

Materials and Methods

Animals. Eight-to-ten weeks old C57BL/6NCRL mice and 14 to 15 wk old LEW/Crl rats were purchased from Charles River Laboratories and housed under a 12-h light/dark cycle and temperature ranging 20 to 23 °C with ad libitum access to food and water. For the PPMS model, adult female C57BL/6 J mice were purchased from The Jackson Laboratory (Bar Harbor, ME). All procedures were approved by the IACUC at Mispro Biotech Services (New York) or Neuron23 IACUC (South San Francisco).

Compounds. Compounds A and B were identified at Neuron23, and details will be disclosed in due course. BMS-986165 was synthesized according to the literature (69).

IFNα PK/PD. Six- to nine-weeks-old C57BL/6NCRL mice were orally dosed once with test articles (TAs) and stimulated with recombinant IFNα (PBL; 10 ng/g) via IP injection 0.5 h later. Tissues were collected 3 h post-IP injection (3.5 h post-TA dosing).

EAE Induction. Mice were subcutaneously injected with control complete Freund's adjuvant (CFA) (CK-2110, Hooke Laboratories, Lawrence, MA), myelin oligodendrocyte glycoprotein $(MOG)_{35-55}$/CFA (EK-2110) or MOG_{1-125}/CFA (EK-2160) emulsion bilaterally along the lower lumbar dorsal region followed by pertussis toxin IP injection on days 0 and 2 according to the manufacturer's instruction. Rats were subcutaneously injected on day 0 with CFA (EK-3110) or guinea pig myelin basic protein $(gpMBP)_{69-88}$/CFA emulsion bilaterally along the lower lumbar dorsal region according to the manufacturer's instruction. Clinical manifestation of neuromuscular deficits are quantified as described in *SI Appendix*.

PPMS Recombinant Antibody rAb Mouse Model. Human research protocol executed at International Multiple Sclerosis Management Practice under IRB approval by Western Institutional Review Board (WIRB® Protocol #20152309). All participants provided informed consent in accordance with the Declaration of Helsinki. PPMS patient-derived recombinant antibody (rAB) was delivered to adult female C57BL/6 J mice as depicted in Fig. 6*A* and previously described (41). Additional details in *SI Appendix*. Mice were randomly assigned to treatment groups. All motor testing was performed blinded with respect to treatment groups. Following intrathecal delivery of PPMS rAbs, mice underwent motor testing at 1 DPI and 3 DPI. Forelimb reaching, gripping, and tail flaccidity were evaluated on a 3-point scale as described in *SI Appendix*.

Animal Treatment. For the semitherapeutic paradigm, treatments were initiated en masse when 20% of MOG-induced animals showed a clinical score of 0.5. Cohorts were balanced based on clinical score prior to start of treatment. For therapeutic paradigm, animals were enrolled individually into a dosing arm when

scoring at least 0.5. Animals were distributed to each dosing group in a balanced fashion based on clinical score. Enrollment was closed 16 d post induction, and experiments were concluded 28 d post enrollment. For prophylactic paradigm, treatments were initiated one day prior to injection of PPMS rAb. Test article formulation and treatment methods described in *SI Appendix*.

Flow Cytometry T Cell and B Cell Quantification. Terminal whole blood was collected via cardiac puncture and following perfusion, hemibrain collected, and processed according to Multi Tissue Dissociation Kit 1 (130-110-201) instructions using a gentleMACS Octo Dissociator with heaters (Miltenyi Bio, 130-096-427) per manufacturer instructions. Additional sample processing and antibody staining methods described in *SI Appendix*.

Anti-MOG IgG Quantification. Total terminal plasma MOG_{1-125} IgG was quantified using a commercially available anti-MOG_{1-125} mouse IgG ELISA kit (AS-55153-M, AnaSpec).

Immunohistochemistry. For MOG_{1-125} immunogen EAE, a subset of animals (n = 3 per group) was selected for immunohistochemical processing. These animals were selected from each group in a balanced fashion based on terminal clinical score and overall clinical deficit. IHC processing, staining, and imaging was performed by NeuroScience Associate (Knoxville, TN) and described in *SI Appendix*. For rAB-induced PPMS model, all samples (n = 6 per group) were processed and analyzed by IHC at Tisch MS Research Center, as described in *SI Appendix*.

RNAscope In Situ Hybridization Assay. RNAscope is an RNA in situ hybridization (ISH) technology developed and performed by Advanced Cell Diagnostics (ACD Bio; Newark, CA). Briefly, the RNAscope 2.5 LS multiplex fluorescent ISH assay was utilized for the detection of *Tyk2, Aif1, Gfap*, and *Rbfox3* messenger RNA (mRNA) in three wild-type mouse sagittal brain hemispheres, as described in *SI Appendix*.

Gene Expression Analysis. Gene expression analysis of tissues collected was performed and visualized as described in *SI Appendix*.

Cytokine/Chemokine Analysis. Cytokines, chemokines, and neurofilament light polypeptide (NfL) (MSD, K1517XR-2) were measured in plasma, spinal cord, brain, or iAstrocytes using the MSD U-PLEX system or R-plex assay. Snap-frozen brains and spinal cords were homogenized in 1x MSD Lysis Buffer supplemented with complete protease (Sigma Aldrich, 5892970001) and PhosSTOP phosphatase inhibitor (Sigma Aldrich, 4906837001) using soft-tissue ceramic beads (Precellys, CK14) and a bead homogenizer (MP Bio, FastPrep-24 5G). Plasma and tissue lysates were diluted in MSD assay diluent and run as per manufacturer instructions.

Biochemical Assays. Kinase-domain (JH1) enzymatic assays:

JAK-family JH1 domain enzymatic inhibition assays were performed by Pharmaron (Beijing, CHN), as described in *SI Appendix*.

Pseudokinase-domain (JH2) Kd determination:

JAK-family JH2 domain binding affinities were determined by Eurofins DiscoverX (San Diego) according to previously published methodology (70).

Cell Culture and Phosphorylated STAT Activity Assays. THP-1 cells (ATCC, TIB-202) and human iPSC-derived astrocytes (BrainXcell, BX-0600) and microglia (iMicroglia) (BX-0900) were cultured and stimulated with cytokines as described in *SI Appendix*. Analyses of pSTAT activity were performed using AlphaLISA or MSD according to the manufacturer's protocol. Custom pTyr1054/1055 TYK2 and total TYK2 MSD assays were performed to measure direct target engagement.

To generate reactive astrocytes, cells were stimulated on day 4 with media containing Tumor Necrosis Factor Alpha (TNF-a) (30 ng/ml, R&D Systems, 210-TA-020), IL-1a (3 ng/ml, Sigma, 13901), and C1q (400 ng/ml, Abcam, AB282858) (TIC) or combinations of TIC with human IFN-β (100 ng/ml, PBL Assay Science, 11415). Conditioned medium was collected posttreatment at 24- or 48-h for chemokine/cytokine MSD assay and cell pellets were saved for gene signature analysis.

Western blot. Western blot analysis of total TYK2 and pTyr1054/1055 TYK2 in iAstrocytes and iMicroglia was performed as described in *SI Appendix*.

Data, Materials, and Software Availability. All study data are included in the article and/or *SI Appendix*.

1. S. Banerjee, A. Biehl, M. Gadina, S. Hasni, D. Schwartz, JAK–STAT signaling as a target for inflammatory and autoimmune diseases: Current and future prospects. *Drugs* **77**, 521–546 (2017).
2. L. T. Jensen, K. E. Attfield, M. Feldmann, L. Fugger, Allosteric TYK2 inhibition: Redefining autoimmune disease therapy beyond JAK1-3 inhibitors. *EBioMedicine* **97**, 104840 (2023), 10.1016/j.ebiom.2023.104840.
3. F. M. Pellenz *et al.*, Association of TYK2 polymorphisms with autoimmune diseases: A comprehensive and updated systematic review with meta-analysis. *Genet Mol. Biol.* **44**, e20200425 (2021), 10.1590/1678-4685-gmb-2020-0425.
4. J.-H. Tao *et al.*, Meta-analysis of TYK2 gene polymorphisms association with susceptibility to autoimmune and inflammatory diseases. *Mol. Biol. Rep.* **38**, 4663–4672 (2011).
5. S. T. Wrobleski *et al.*, Highly selective inhibition of tyrosine kinase 2 (TYK2) for the treatment of autoimmune diseases: Discovery of the allosteric inhibitor BMS-986165. *J. Med. Chem.* **62**, 8973–8995 (2019).
6. M. Uhlén *et al.*, Tissue-based map of the human proteome. *Science* **347**, 1260419 (2015).
7. Inger-Lise. Mero *et al.*, A rare variant of the TYK2 gene is confirmed to be associated with multiple sclerosis. *Eur. J. Hum. Genet* **18**, 502–504 (2010).
8. Maria Ban *et al.*, Replication analysis identifies TYK2 as a multiple sclerosis susceptibility factor. *Eur. J. Hum. Genet.* **17**, 1309–1313 (2009).
9. N. Couturier *et al.*, Tyrosine kinase 2 variant influences T lymphocyte polarization and multiple sclerosis susceptibility. *Brain* **134**, 693–703 (2011).
10. C. A. Dendrou *et al.*, Resolving TYK2 locus genotype-to-phenotype differences in autoimmunity. *Sci. Transl. Med.* **8**, RA363 (2016).
11. A. Oyamada *et al.*, Tyrosine kinase 2 plays critical roles in the pathogenic CD4 T cell responses for the development of experimental autoimmune encephalomyelitis. *J. Immunol.* **183**, 7539–7546 (2009).
12. J. A. Gorman *et al.*, The TYK2-P1104A autoimmune protective variant limits coordinate signals required to generate specialized T cell subsets. *Front Immunol.* **10**, 44 (2019).
13. J. R. Burke *et al.*, Autoimmune pathways in mice and humans are blocked by pharmacological stabilization of the TYK2 pseudokinase domain. *Sci. Transl. Med.* **11**, EAAW1736 (2019).
14. G. Giovannoni *et al.*, Smouldering multiple sclerosis: The 'real MS'. *Ther. Adv. Neurol. Disord* **15**, 17562864211066751 (2022), 10.1177/17562864211066751.
15. B. A. Hart, A. Luchicchi, G. J. Schenk, P. K. Stys, J. J. G. Geurts, Mechanistic underpinning of an inside–out concept for autoimmunity in multiple sclerosis. *Ann. Clin. Transl. Neurol.* **8**, 1709–1719 (2021).
16. L. Velazquez, M. Fellous, G. R. Stark, S. Pellegrini, A protein tyrosine kinase in the interferon αβ signaling pathway. *Cell* **70**, 313–322 (1992).
17. C. Lütticken *et al.*, Association of transcription factor APRF and protein kinase Jak1 with the interleukin-6 signal transducer gp130. *Science* **263**, 89–92 (1994).
18. N. Stahl *et al.*, Association and activation of Jak-Tyk kinases by CNTF-LIF-OSM-IL-6 β receptor components. *Science* **263**, 92–95 (1994).
19. L. S. Argetsinger *et al.*, Identification of JAK2 as a growth hormone receptor–associated tyrosine kinase. *Cell* **74**, 237–244 (1993).
20. B. A. Witthuhn *et al.*, JAK2 associates with the erythropoietin receptor and is tyrosine phosphorylated and activated following stimulation with erythropoietin. *Cell* **74**, 227–236 (1993).
21. M. C. Gauzzi *et al.*, Interferon-α-dependent activation of Tyk2 requires phosphorylation of positive regulatory tyrosines by another kinase. *J. Biol. Chem.* **271**, 20494–20500 (1996).
22. E. Yang, M. M. H. Li, All about the RNA: Interferon-stimulated genes that interfere with viral RNA processes. *Front Immunol.* **11**, 605024 (2020).
23. A. Murira, A. Lamarre, Type-I interferon responses: From friend to foe in the battle against chronic viral infection. *Front Immunol.* **7**, 609 (2016).
24. J.-A. Lyons, M. San, M. P. Happ, A. H. Cross, B cells are critical to induction of experimental allergic encephalomyelitis by protein but not by a short encephalitogenic peptide. *Eur. J. Immunol.* **29**, 3432–3439 (1999).
25. S. Srinivasan *et al.*, Transcriptional dysregulation of Interferome in experimental and human multiple sclerosis. *Sci. Rep.* **7**, 09286 (2017), 10.1038/s41598-017-09286-y.
26. A. Montilla *et al.*, Microglia and meningeal macrophages depletion delays the onset of experimental autoimmune encephalomyelitis. *Cell Death Dis.* **14**, 16 (2023), 10.1038/s41419-023-05551-3.
27. H. S. Kwon, S.-H. Koh, Neuroinflammation in neurodegenerative disorders: The roles of microglia and astrocytes. *Transl. Neurodegener* **9**, 42 (2020).
28. Z. Jie *et al.*, Microglia promote autoimmune inflammation via the noncanonical NF-κB pathway. *Sci. Adv.* **7**, abh0609 (2021), 10.1126/sciadv.abh0609.
29. B. Bonetti *et al.*, Activation of NF-kappaB and c-jun transcription factors in multiple sclerosis lesions. Implications for oligodendrocyte pathology. *Am. J. Pathol.* **155**, 1433–1438 (1999).
30. J. Yan, J. M. Greer, NF-?B, a potential therapeutic target for the treatment of multiple sclerosis *CNS Neurol. Disord Drug Targets* **7**, 536–557 (2008).
31. C. Mc Guire, M. Prinz, R. Beyaert, G. van Loo, Nuclear factor kappa B (NF-@kB) in multiple sclerosis pathology. *Trends Mol. Med.* **19**, 604–613 (2013).
32. Y. Yue, S. Stone, W. Lin, Role of nuclear factor κB in multiple sclerosis and experimental autoimmune encephalomyelitis. *Neural Regen. Res.* **13**, 1507–1515 (2018).
33. B. Hilliard, E. B. Samoilova, T.-S.T. Liu, A. Rostami, Y. Chen, Experimental autoimmune encephalomyelitis in NF-κB- deficient mice: Roles of NF-κB in the activation and differentiation of autoreactive T cells. *J. Immunol.* **163**, 2937–2943 (1999).
34. B. Greve *et al.*, I B kinase 2/ deficiency controls expansion of autoreactive T cells and suppresses experimental autoimmune encephalomyelitis. *J. Immunol.* **179**, 179–185 (2007).
35. T. Kawai, S. Akira, The role of pattern-recognition receptors in innate immunity: Update on Toll-like receptors. *Nat. Immunol.* **11**, 373–384 (2010).
36. T. Kawai, S. Akira, Signaling to NF-@kB by Toll-like receptors. *Trends Mol. Med.* **13**, 460–469 (2007).
37. L. M. Pfeffer, The role of nuclear factor? B in the interferon response *J. Interferon Cytokine Res.* **31**, 553–559 (2011).

38. J. Åkesson *et al.*, Proteomics reveal biomarkers for diagnosis, disease activity and long-term disability outcomes in multiple sclerosis. *Nat. Commun.* **14**, 6903 (2023), 10.1038/s41467-023-42682-9.
39. Z. Bai *et al.*, Cerebrospinal fluid and blood cytokines as biomarkers for multiple sclerosis: A systematic review and meta-analysis of 226 studies with 13,526 multiple sclerosis patients. *Front. Neurosci.* **13**, 1026 (2019).
40. W. J. Karpus, Cytokines and chemokines in the pathogenesis of experimental autoimmune encephalomyelitis. *J. Immunol.* **204**, 316–326 (2020).
41. J. K. Wong *et al.*, Cerebrospinal fluid immunoglobulins in primary progressive multiple sclerosis are pathogenic. *Brain* **146**, 1979–1992 (2023).
42. Z. Haimon *et al.*, Cognate microglia–T cell interactions shape the functional regulatory T cell pool in experimental autoimmune encephalomyelitis pathology. *Nat. Immunol.* **23**, 1749–1762 (2022).
43. M. M. Mielke *et al.*, Plasma and CSF neurofilament light: Relation to longitudinal neuroimaging and cognitive measures. *Neurology* **93**, e252–e260 (2019), 10.1212/WNL.0000000000007767.
44. L. Ning, B. Wang, Neurofilament light chain in blood as a diagnostic and predictive biomarker for multiple sclerosis: A systematic review and meta-analysis. *PLoS One* **17**, E274565 (2022).
45. P. Prakash *et al.*, Proteomic profiling of interferon-responsive reactive astrocytes in rodent and human. *Glia* **72**, 625–642 (2024).
46. S. A. Liddelow *et al.*, Neurotoxic reactive astrocytes are induced by activated microglia. *Nature* **541**, 481–487 (2017).
47. L. Barbar *et al.*, CD49f is a novel marker of functional and reactive human iPSC-derived astrocytes. *Neuron* **107**, 436–453 (2020).
48. C. L. Langrish *et al.*, IL-23 drives a pathogenic T cell population that induces autoimmune inflammation. *J. Exp. Med.* **201**, 233–240 (2005).
49. B. Becher, B. G. Durell, R. J. Noelle, Experimental autoimmune encephalitis and inflammation in the absence of interleukin-12. *J. Clin. Invest.* **110**, 493–497 (2002).
50. B. Gran *et al.*, IL-12p35-deficient mice are susceptible to experimental autoimmune encephalomyelitis: Evidence for redundancy in the IL-12 system in the induction of central nervous system autoimmune demyelination. *J. Immunol.* **169**, 7104–7110 (2002).
51. R. Amoriello, C. Memo, L. Ballerini, C. Ballerini, The brain cytokine orchestra in multiple sclerosis: From neuroinflammation to synaptopathology. *Mol. Brain* **17**, 4 (2024), 10.1186/s13041-024-01077-7.
52. X. Yu, M. Graner, P. G. E. Kennedy, Y. Liu, The role of antibodies in the pathogenesis of multiple sclerosis. *Front. Neurol.* **11**, 533388 (2020).
53. I. Marié, J. E. Durbin, D. E. Levy, Differential viral induction of distinct interferon-α genes by positive feedback through interferon regulatory factor-7. *EMBO J.* **17**, 6660–6669 (1998).
54. M. Sato *et al.*, Positive feedback regulation of type I IFN genes by the IFN-inducible transcription factor IRF-7. *FEBS Lett.* **441**, 106–110 (1998).
55. D. S. Skundric, W. W. Cruikshank, J. Drulovic, Role of IL-16 in CD4+ T cell-mediated regulation of relapsing multiple sclerosis *J. Neuroinflammation* **12**, 78 (2015), 10.1186/s12974-015-0292-x.
56. D. S. Skundric, J. Cai, W. W. Cruikshank, D. Gveric, Production of IL-16 correlates with CD4+ Th1 inflammation and phosphorylation of axonal cytoskeleton in multiple sclerosis lesions *J. Neuroinflammation* **3**, 13 (2006).
57. S. U. Hridi *et al.*, Increased levels of IL-16 in the central nervous system during neuroinflammation are associated with infiltrating immune cells and resident glial cells. *Biology (Basel)* **10**, 472 (2021), 10.3390/biology10060472.
58. E. Martynova *et al.*, Serum and cerebrospinal fluid cytokine biomarkers for diagnosis of multiple sclerosis. *Mediators Inflamm.* **2020**, 2727042 (2020).
59. J. Huang *et al.*, Inflammation-related plasma and CSF biomarkers for multiple sclerosis. *Proc. Natl. Acad. Sci. U.S.A.* **117**, 12952–12960 (2020).
60. K. E. Balashov, J. B. Rottman, H. L. Weiner, W. W. Hancock, CCR5+ and CXCR3+ T cells are increased in multiple sclerosis and their ligands MIP-1α and IP-10 are expressed in demyelinating brain lesions *Proc. Natl. Acad. Sci. U.S.A.* **96**, 6873–6878 (1999).
61. J. M. Lawrence, K. Schardien, B. Wigdahl, M. R. Nonnemacher, Roles of neuropathology-associated reactive astrocytes: A systematic review. *Acta Neuropathol. Commun.* **11**, 42 (2023), 10.1186/s40478-023-01526-9.
62. P. Hasel, W. H. Aisenberg, F. C. Bennett, S. A. Liddelow, Molecular and metabolic heterogeneity of astrocytes and microglia. *Cell Metab.* **35**, 555–570 (2023).
63. R. Dobson, R. A. Rudick, B. Turner, K. Schmierer, G. Giovannoni, Assessing treatment response to interferon-β: Is there a role for MRI? *Neurology* **82**, 248–254 (2014).
64. J. Río *et al.*, Assessment of different treatment failure criteria in a cohort of relapsing–remitting multiple sclerosis patients treated with interferon β: Implications for clinical trials. *Ann. Neurol.* **52**, 400–406 (2002).
65. X. Feng *et al.*, Interferon-β corrects massive gene dysregulation in multiple sclerosis: Short-term and long-term effects on immune regulation and neuroprotection. *EBioMedicine* **49**, 269–283 (2019).
66. H. Hegen *et al.*, Cytokine profiles show heterogeneity of interferon-β response in multiple sclerosis patients. *Neurol. Neuroimmunol. Neuroinflamm.* **3**, e202 (2016), 10.1212/NXI.0000000000000202.
67. R. C. Axtell *et al.*, T helper type 1 and 17 cells determine efficacy of interferon-ß in multiple sclerosis and experimental encephalomyelitis. *Nat. Med.* **16**, 406–412 (2010).
68. A. Agasing, J. L. Quinn, G. Kumar, R. C. Axtell, Interferon-β intensifies interleukin-23-driven pathogenicity of T helper cells in neuroinflammatory disease. *Cells* **10**, 2139 (2021), 10.3390/cells10082139.
69. R. Moslin *et al.*, Identification of N-methyl nicotinamide and N-methyl pyridazine-3-carboxamide pseudokinase domain ligands as highly selective allosteric inhibitors of tyrosine kinase 2 (TYK2). *J. Med. Chem.* **62**, 8953–8972 (2019).
70. M. A. Fabian *et al.*, A small molecule–kinase interaction map for clinical kinase inhibitors. *Nat. Biotechnol.* **23**, 329–336 (2005).